

1 **GPUMCD: a new GPU-Oriented Monte Carlo dose calculation**
2 **platform**

3 Sami Hissoiny* and Benoît Ozell

4 *École polytechnique de Montréal, Département de génie informatique et génie logiciel,*
5 *2500 chemin de Polytechnique. Montréal (Québec), CANADA H3T 1J4*

6 Hugo Bouchard and Philippe Després

7 *Département de Physique, Université de Montréal,*
8 *Pavillon Roger-Gaudry (D-428), 2900 Boulevard Édouard-Montpetit,*
9 *Montréal, Québec H3T 1J4, Canada and Département de Radio-oncologie,*
10 *Centre hospitalier de l'Université de Montréal (CHUM),*
11 *1560 Sherbrooke est, Montréal, Québec H2L 4M1, Canada*

12 (Dated: May 28, 2018)

Abstract

Purpose : Monte Carlo methods are considered the gold standard for dosimetric computations in radiotherapy. Their execution time is however still an obstacle to the routine use of Monte Carlo packages in a clinical setting. To address this problem, a completely new, and designed from the ground up for the GPU, Monte Carlo dose calculation package for voxelized geometries is proposed: GPUMCD.

Method : GPUMCD implements a coupled photon-electron Monte Carlo simulation for energies in the range 0.01 MeV to 20 MeV. An analogue simulation of photon interactions is used and a Class II condensed history method has been implemented for the simulation of electrons. A new GPU random number generator, some divergence reduction methods as well as other optimization strategies are also described. GPUMCD was run on a NVIDIA GTX480 while single threaded implementations of EGSnrc and DPM were run on an Intel Core i7 860.

Results : Dosimetric results obtained with GPUMCD were compared to EGSnrc. In all but one test case, 98% or more of all significant voxels passed a gamma criteria of 2%-2mm. In terms of execution speed and efficiency, GPUMCD is more than 900 times faster than EGSnrc and more than 200 times faster than DPM, a Monte Carlo package aiming fast executions. Absolute execution times of less than 0.3 s are found for the simulation of 1M electrons and 4M photons in water for monoenergetic beams of 15 MeV, including GPU-CPU memory transfers.

Conclusion : GPUMCD, a new GPU-oriented Monte Carlo dose calculation platform, has been compared to EGSnrc and DPM in terms of dosimetric results and execution speed. Its accuracy and speed make it an interesting solution for full Monte Carlo dose calculation in radiation oncology.

¹³ Keywords: Monte Carlo, GPU, CUDA, EGSnrc, DPM, DOSXYZnrc,

* sami.hissoiny@polymtl.ca

14 I. INTRODUCTION

15 Monte Carlo packages such as EGS4 [1], EGSnrc [2, 3], EGS5 [4] and PENELOPE [5, 6]
16 have been extensively compared to experimental data in a large array of conditions, and
17 generally demonstrate excellent agreement with measurements. EGSnrc, for instance, was
18 shown to “pass the Fano cavity test at the 0.1% level” [7]. Despite this accuracy, Monte
19 Carlo platforms are mostly absent from routine dose calculation in radiation therapy due to
20 the long computation time required to achieve sufficient statistical significance.

21 Monte Carlo simulations are generally considered the gold standard for benchmarking
22 analytical dose calculation approaches such as pencil-beam based computations [8–10] and
23 convolution-superposition techniques [11, 12]. Such techniques typically use precomputed
24 Monte Carlo data to incorporate physics-rich elements in the dose calculation process. These
25 semi-empirical methods were developed as a trade-off between accuracy and computation
26 time and as such do not match the level of accuracy offered by Monte Carlo simulations,
27 especially in complex heterogeneous geometries where differences of up to 10% were re-
28 ported [13–15].

29 Fast Monte Carlo platforms have been developed for the specific purpose of radiotherapy
30 dose calculations, namely VMC [16–18] and DPM [19]. These packages make some sacrifices
31 to the generality and absolute accuracy of the simulation by, for example, restricting the
32 energy range of incoming particles. This assumption allows simpler treatment of certain
33 particle interactions which are less relevant within the limited energy range considered.
34 Gains in efficiency of around 50 times can be achieved by these packages when compared to
35 general-purpose solutions.

36 This paper presents GPUMCD (GPU Monte Carlo Dose), a new code that follows the
37 fast Monte Carlo approach. GPUMCD relies on a relatively new hardware platform for
38 computations: the GPU (Graphics Processing Unit). The GPU is gaining momentum in
39 medical physics [20–23] as well as in other spheres [24–28] where high-performance computing
40 is required. A layer-oriented simulation based on the MCML Monte Carlo code for photon
41 transport has already been ported to the GPU [29]. The photon transport algorithm from
42 PENELOPE has also been ported to the GPU [30] for accelerations of up to 27x. DPM [19]
43 has been ported to the GPU with excellent dosimetric results compared to the CPU version,
44 as expected, but with relatively low (5-6.6x) acceleration factors [31].

45 A comparison of GPUMCD to the work by Jia *et al.* must be made cautiously. The work
46 of Jia *et al.* is a port of an existing algorithm that is not, to the best of our knowledge,
47 designed for the specific nature of the GPU. Notable differences are found between the two
48 approaches regarding the treatment of secondary particles and the electron-photon coupling.
49 These differences will be exposed in Sec. II C 3. The code presented in this article is the first
50 attempt of a complete rewrite of a coupled photon-electron Monte Carlo code specifically
51 designed for the GPU. New techniques for the memory management of particles as well
52 as efforts to reduce the inherent divergent nature of Monte Carlo algorithms are detailed.
53 Divergence in GPU programming arises from conditional branching, which is not optimal
54 in stream processing where predictable execution is expected for optimal performances. No
55 new sampling methods used in Monte Carlo simulations were introduced in GPUMCD; all
56 theoretical developments of cross section sampling methods have been adapted from their
57 description in general-purpose Monte Carlo package manuals (and references therein) listed
58 previously. However, their actual implementation is original, as it is specifically tailored
59 for parallel execution on graphics hardware, and the code has not been taken from existing
60 Monte Carlo implementations.

61 The paper is structured as follows: Sec. II introduces the physics principles as well as
62 the hardware platform and implementation details. Sec. III presents the results in terms of
63 dose and calculation efficiency of GPUMCD compared to the EGSnrc and DPM platforms.
64 Finally, a discussion of the reported results is presented in Sec. IV.

65 II. MATERIAL AND METHODS

66 A. Photons simulation

67 Photon transport can be modeled with an analogue simulation, *i.e.* every interaction
68 is modeled independently until the particle leaves the geometry or its energy falls below a
69 certain energy level referenced as P_{cut} from now on. This allows for an easy implementation
70 of the transport process.

71 GPUMCD takes into account Compton scattering, the photoelectric effect and pair pro-
72 duction. Rayleigh scattering can be safely ignored for the energy range considered (10 keV-
73 20 MeV). Considering a homogeneous phantom, the distance to the next interaction, noted

74 s , can be sampled from the following expression:

$$s = -\frac{1}{\mu(E)} \ln(\zeta), \quad (1)$$

75 where ζ is a random variable uniformly distributed in $(0,1]$ and $\mu(E)$ is the value of the total
76 attenuation coefficient, given by

$$\mu = \frac{N_A}{A} \rho (\sigma_{compton} + \sigma_{photo} + \sigma_{pair}), \quad (2)$$

77 where the σ 's are total cross section values for the corresponding interactions, N_A is Avo-
78 gadro's number, A is the molecular weight and ρ is the density.

79 To eliminate the need for a distinct geometry engine in heterogeneous situations,
80 GPUMCD employs the Woodcock raytracing algorithm [32] in which the volume can be
81 considered homogeneously attenuating by introducing a fictitious attenuation coefficient,
82 corresponding to a fictitious interaction which leaves the direction and energy of the particle
83 unchanged, in every voxel \vec{x} :

$$\mu(\vec{x})_{fict} = \mu_{max} - \mu(\vec{x}) \quad (3)$$

84 where μ_{max} is the attenuation coefficient of the most attenuating voxel inside the volume.
85 The distance to the next interaction is therefore always sampled using μ_{max} . The sampling
86 of the interaction type, once at the interaction position, is then performed taking into
87 consideration this fictitious interaction type. This method is not an approximation, it leads
88 to the correct result even in arbitrarily heterogeneous geometries.

89 Compton scattering is modeled with a free electron approximation using the Klein-Nishina
90 cross section [33]. The energy and direction of the scattered photon and secondary electron
91 are sampled according to the direct method derived by Everett *et al.* [34]. Binding effects and
92 atomic relaxation are not modeled. These approximations are reasonable when the particle
93 energy is large compared to the electron binding energy which is the case for radiation
94 therapy [35].

95 The photoelectric effect is modeled by once again ignoring atomic relaxation. Addition-
96 ally, shell sampling is also ignored and all electrons are assumed to be ejected from the
97 K-shell. The sole product of the interaction is a new electron in motion with total energy
98 $E_{elec} = E_{phot}$. The angular sampling of the electron is selected according to the Sauter
99 distribution [36] following the sampling formula presented in Sec. 2.2 of the PENELOPE

100 manual [5]. The simulation of the photoelectric effect will become less accurate when the
101 energy of the photon is in the order of the characteristic X-ray radiation energy of the mate-
102 rial since characteristic X-rays are not produced. Therefore, at the previously stated lower
103 energy range threshold of 10 keV, photons are still tracked and simulated but the accu-
104 racy of the simulation of the photoelectric effect will be dependent on the material where
105 the simulation is taking place. The binding energies being low in organic compound, this
106 approximation is considered acceptable.

107 Relatively crude approximations are employed when simulating pair production events.
108 First and foremost, no positrons are simulated in this package. The pair production event
109 instead generates two secondary electrons. The relatively low probability of pair production
110 events at the energies considered as well as the additional low probability of in-flight an-
111 nihilation of the positron make this approximation suitable [19]. Triplet production is also
112 not modeled. The energy of the incoming photon is trivially split between the two electrons
113 using a uniformly distributed random number. The angle of both electrons is sampled using
114 the algorithm presented in Eq. 2.1.18 of the EGSnrc manual [37].

115 B. Electron simulation

116 Because of the much larger number of interactions experienced by a charged particle be-
117 fore it has deposited all of its energy, analogue simulations cannot be used practically. A
118 class II condensed history method is used here, as defined by Berger [38], in which inter-
119 actions are simulated explicitly only if they cause a change in orientation greater than θ_c
120 or a change in energy larger than E_c . Below these thresholds, the interactions are modeled
121 as taking part of a larger condensed interaction, the result of which is a major change in
122 direction and energy. Above the thresholds, interactions, usually called hard or catastrophic
123 interactions, are modeled in an analogue manner similar to the simulation of photons.

124 1. Hard interactions

125 GPUMCD simulates inelastic collisions as well as bremsstrahlung in an analogue manner,
126 as long as the changes to the state of the particle are greater than the previously discussed
127 threshold.

128 For inelastic collisions, a free electron approximation is used and no electron impact
 129 ionization nor spin effects are modeled. The Møller cross section is used to describe the
 130 change in energy and direction of the scattered and knock-on electrons. The sampling
 131 routine presented in Sec. 2.4.3.i of the EGSnrc manual [37] is used.

132 During a bremsstrahlung event, the energy of the created photon is sampled as presented
 133 in Sec. 2.4.2.ii of the EGSnrc manual. Approximations to the angular events are employed :
 134 the angle of the electron is unchanged and the angle of the photon is selected as $\theta = m_0c^2/E$
 135 where E is the energy of the incoming electron.

136 2. Multiple scattering

137 The class II condensed history method requires the selection of an angle for the multiply-
 138 scattered electron after a step, as discussed in the next subsection. To this end, the formu-
 139 lation presented by Kawrakow and Bielajew [39] and Kawrakow [2] is used. The required
 140 q_{SR}^{2+} data are imported from the `msnew.dat` file packaged with EGSnrc.

141 3. Electrons transport

142 The transport of electrons is less straightforward than photon transport because of the
 143 high probability of soft collisions, which are regrouped in a single step between two hard inter-
 144 actions (collision or bremsstrahlung events). This condensed history method introduces an
 145 unphysical (but mathematically converging) factor for the length of the multiple-scattering
 146 step. Between consecutive hard collisions, which are separated by a distance sampled with an
 147 electron version of Eq. (1), a number of multiple-scattering events will occur. In GPUMCD,
 148 a simple step-length selection (henceforth e_s) is used and can be summarized as

$$e_s = \min\{d_{vox}, e_{s-max}, e_{hard}\} \quad (4)$$

149 where d_{vox} is the distance to the next voxel boundary, e_{s-max} is a user-supplied upper bound
 150 of step length and e_{hard} is the distance to the next hard interaction.

151 The distance to the next hard interaction can once again be sampled with the help of
 152 the Woodcock raytracing algorithm. For electron transport, however, the total attenuation
 153 coefficient, $\mu(E)$, is in fact $\mu(E, s)$ where the dependence on distance has been made explicit.

154 The dependence on distance is due to the fact that electrons will lose energy due to sub-
 155 threshold interactions between two successive hard interactions. In this application, the
 156 approximation is made that the attenuation coefficient is decreasing with respect to the
 157 particle energy. It is not rigorously true, as shown in [2], but allows for an easier treatment
 158 since $\mu_{max}(E)$ can be selected with E being the energy at the beginning of the electron step.

159 Energy losses are experienced by the electron during the soft scattering events that are
 160 modeled by the multiple-scattering step. This energy loss is accounted for with the con-
 161 tinuously slowing down approximation (CSDA). This approximation states that charged
 162 particles are continuously being slowed down due to the interactions they go through and
 163 that the rate of energy loss is equal to the stopping power S , given by:

$$S(E) = -\frac{dE}{ds}. \quad (5)$$

164 The implementation of a class II condensed history method only accounts for sub-threshold
 165 interactions in the CSDA. The use of restricted stopping powers, L , is therefore required:

$$L(E, K_{cut}) = \int_0^{K_{cut}} \Sigma(E, E') dE' \quad (6)$$

166 where $\Sigma(E, E')$ is the total macroscopic cross section and K_{cut} is the catastrophic interaction
 167 kinetic energy threshold. Since this release of GPUMCD is e_s -centric, the energy loss of a
 168 given step is computed with

$$\Delta E = \int_0^{e_s} L(s) ds. \quad (7)$$

169 The evaluation of the integral can be reduced to

$$\Delta E = L(E_0 - L(E_0)s/2) \quad (8)$$

170 which is EGSnrc's Eq. 4.11.3.

171 Between two consecutive hard collisions, the electron does not follow a straight line.
 172 Bielajew's alternate random hinge method [5] builds on PENELOPE's random hinge method
 173 to handle the angular deflection and lateral displacement experienced by an electron during
 174 an electron step. The random hinge method can be described as follows: the electron is
 175 first transported by ζe_s (where ζ is again a uniformly distributed random number), at which
 176 point the electron is rotated by the sampled multiple-scattering angle described in Sec. II B 2
 177 and the energy loss is deposited. The electron is then transported for the remaining distance
 178 equal to $(\zeta - 1)e_s$. Bielajew's refinement of the algorithm involves randomly sampling the

179 angular deflection either before or after the electron has deposited the energy associated
180 with the step.

181 C. GPU implementation

182 In this section, different aspects of the GPU implementation are detailed. GPUMCD is
183 built with the CUDA framework from NVIDIA. A general description of the GPU building
184 blocks and memory levels can be found in [40]. Sec. II C 1 presents the random number
185 generator used in this work while Sec. II C 2 describes the memory management. Finally,
186 Sec. II C 3 addresses the SIMD divergence issue and presents solutions as well as other
187 optimizations used in GPUMCD.

188 1. Random number generator

189 A pseudo random number generator (PRNG) is already available in the NVIDIA SDK
190 (Software Development Kit) for GPU computing. However, it uses a lot of resources which
191 would then be unavailable for the rest of the Monte Carlo simulation. For this reason, a
192 new lightweight PRNG based on the work of Marsaglia [41] was implemented. We use a
193 combined multiply-with-carry (MWC) generator, with recurrence of the form

$$x_{n+1} = (a * x_n + c_n) \bmod (b) \quad (9)$$

194 where a is the multiplier and b the base. The carry, c , is defined by:

$$c_{n+1} = \lfloor \frac{(a * x_n + c_n)}{b} \rfloor. \quad (10)$$

195 The carry c is naturally computed with integer arithmetic and bases b of 2^{32} or 2^{16} . The
196 choice of the multiplier a is not arbitrary: the multiplier is chosen so that $ab - 1$ is safe
197 prime. The period of the PRNG with such a multiplier is on the order of $(ab - 1)/2$. This
198 PRNG has the advantage of using a small amount of registers. By combining two of these
199 generators for each thread, the PRNG uses two 32 bits values for the multipliers and two
200 32 bits values for the current state. Ten integer operations (3 *shifts*, 2 *ands*, 2 *mults* and
201 3 *adds*) are required to generate one new number. It has been shown to pass all tests but
202 one of the TestU01 suite [42], a program designed to test the quality of pseudo random
203 numbers, and to achieve 96.7% of the peak integer bandwidth.

205 GPUMCD is composed of four main arrays: a list of electrons and a list of photons,
206 an array to store composition identifiers and another for density values corresponding to a
207 numerical phantom. During the initialization phase, a call to the `initParticle` function
208 is made which fills the correct particle array (depending on the source particle type) and
209 according to the source type (*e.g.* with a parallel beam source all particles have a direction
210 vector of (0,-1,0)). The particle arrays are allocated only once, with size `MAXSIZE`. The
211 choice of `MAXSIZE` is graphics card dependent as the particle arrays occupy the better part
212 of the global memory, the largest pool of memory on the graphics card. For instance, on
213 a 1 Gb card, `MAXSIZE` could be set to 2^{20} . Only a fraction of the particle array will be
214 filled with source particles, to leave room for secondary particle creation. If for instance
215 `MAXSIZE/d` particles are generated, then each primary particle can generate an average of d
216 secondary particle without running out of memory. The choice of d is therefore important;
217 it is energy dependent and to a lesser extent geometry dependent. For example, with a
218 monoenergetic 15 MeV beam of photons on a 32 cm deep geometry, a value of $d = 8$ was
219 found to be sufficient to accommodate all secondary particles. A global counter of active
220 particles is kept for both electrons and photons and every time a new particle is added
221 the counter is atomically incremented, until it is equal to `MAXSIZE` after which secondary
222 particles are discarded. If the choice of d and `MAXSIZE` are such that the number of particles
223 generated is lower than `MAXSIZE`, then no particles are discarded. Atomic operations are a
224 mechanism that ensure that two parallel threads cannot write the same memory location at
225 the same time, therefore discarding one thread's modification. Atomic operations are not
226 ideal on parallel hardware but these two integer values, the current number of particles of
227 both types, should be efficiently cached on GF100 class hardware through the use of the
228 GPU-wide 768 Kb of L2 cache. After the initialization phase is completed, the simulation
229 starts by calling the function to simulate the initial particle type. Subsequently, secondary
230 particles of the other type are generated and put inside the particle array for that type.
231 The other type of particle will then be simulated, and so on until a relatively low number of
232 particle is left in the stack. This number is user-selectable and could be set to 0 to simulate
233 every particle. Since a simulation pass always comes with some overhead, it could also be
234 set to a non-zero value to avoid the launching of a simulation pass with few particles to

235 simulate which could have a negligible impact on the final distribution. If this impact is in
236 fact negligible of course depends on the threshold selected. Photons and electrons are never
237 simulated in parallel but instead the particles of the *other* type are placed in their respective
238 array and wait there until the array with the *current* type of particle is exhausted. This, in
239 turn, eliminates the divergence due to the photon-electron coupling. Every time a call to a
240 simulation function for electrons or photons is issued, one can consider that every particle of
241 that type is simulated and that the counter for that type of particle is reset to 0. Sec. II C 3
242 will show some refinements related to the management of particles.

243 The other two main arrays, one of composition identifier and one of density values, are
244 stored as 3D textures since they are used to represent the volume of voxels. 3D textures
245 reside in memory but they can be efficiently cached for 3D data locality. Every time a
246 particle is moved, the composition and density of the current particle voxel are fetched from
247 the 3D textures.

248 Cross section and stopping power data are stored in global memory in the form of a 1D
249 texture. The cross section and stopping power data are preinterpolated on a regular grid
250 with a value at every 1 keV.

251 The shared memory usage is relatively limited in this application. For the electrons
252 simulation, some specific composition attributes are required (*e.g.* Z_V , Z_G , etc., in Tab.
253 2.1 of EGS5) and are stored in shared memory. These data values have not been placed in
254 constant memory since that type of memory is best used when all threads of a warp access
255 the same address, which cannot be guaranteed here since these composition attributes are
256 material dependent. Two particles in different materials would therefore request the constant
257 memory at two different addresses, resulting in serialization. No other use for shared memory
258 has been found since the application is by nature stochastic. For instance, we cannot store
259 a portion of the volume since there is no way to know where all the particles of one thread
260 block will be. Similarly, we cannot store a portion of the cross-section data since there is no
261 way to know in which material and with which energy all the particles of one thread block
262 will be.

264 Every multiprocessor (MP) inside the GPU is in fact a SIMD processor and the SIMD
265 coherency has to be kept at the warp level which is the smallest unit of parallelism and
266 is composed of 32 threads. The Monte Carlo simulation being inherently stochastic, it is
267 impossible to predict which path a given particle will take and it is therefore impossible to
268 regroup particle with the same fate into the same warps. When a warp is divergent, it is
269 split into as many subwarps as there are execution paths, leading to a performance penalty.
270 Divergence can be seen when, *e.g.* two particles of the same warp do not require the same
271 number of interactions before exhaustion or do not interact in the same way. Some software
272 mechanisms can be employed to reduce the impact of divergence.

273 The first mechanism consists in performing a stream compaction after N simulation
274 steps, where N is user-defined and corresponds to a number of interactions for photons and
275 to a number of catastrophic events for electrons. For example, if one particle requires 20
276 interactions to complete and the others in the warp require less than 5, then some scalar
277 processors (SP) in the MP will be idle while they wait for the *slow* particle to finish. This
278 first mechanism then artificially limits the number of simulation steps a particle can undergo
279 during one pass of the algorithm. After this number of steps, every particle that has been
280 completely simulated is removed from the list of particles and the simulation is restarted
281 for another N steps, until every particle has been completely simulated. The removal of
282 particles is not free and therefore it is not clear if this technique will have a positive effect
283 on execution time. The stream compaction is accomplished with the CHAG library [43].

284 A second mechanism, named persistent thread by its creators and *pool* in GPUMCD, is
285 taken from the world of graphics computing [44]. In this approach, the minimum number of
286 threads to saturate the GPU is launched. These threads then select their workload from a
287 global queue of particles to be simulated. Once a thread is done with one particle, it selects
288 the next particle, until all have been simulated. This is once again to reduce the impact of
289 the imbalance in the number of interactions per particle.

290 All the GPU code uses single precision floating point numbers as they offer a significant
291 speed improvement over double precision floating point numbers on graphics hardware. The
292 work of Jia et al. [31] showed that no floating point arithmetic artifacts were introduced for
293 this type of application.

294 A notable difference between this work and the work by Jia *et al.* is the way the secondary
295 particles are treated. In the work by Jia, a thread is responsible for its primary particle as
296 well as every secondary particles it creates. This can be a major source of divergence because
297 of the varying number of secondary particles created. On the other hand, GPUMCD does
298 not immediately simulate secondary particles but instead places them in their respective
299 particle arrays. After a given pass of the simulation is over, the arrays are checked for newly
300 created secondary particles and if secondary particles are found, they are simulated. This
301 eliminates the divergence due to the different number of secondary particles per primary
302 particles. Additionally, since Jia *et al.* use a single thread per primary particles, a thread
303 may be responsible for the simulation of both electrons and photons which can in turn be a
304 major source of divergence. For example, at time t , thread A may be simulating a secondary
305 electron while thread B a secondary photon. In other words, they simulate both photons
306 and electrons at the same time. Since both of these particles most likely have completely
307 different code path, heavy serialization will occur. On the other hand, since GPUMCD
308 stores secondary particles in arrays to be simulated later, no such divergence due to the
309 electron-photon coupling occurs.

310 Finally, GPUMCD can be configured to take advantage of a multi-GPU system. The
311 multi-GPU approach is trivial for Monte Carlo simulations: both GPUs execute the
312 `initParticle` function and simulate their own set of particles. After the simulations,
313 the two resulting dose arrays are summed. Linear performance gains are expected for
314 simulations when there are enough particles to simulate to overcome the overhead penalty
315 resulting from copying input data to two graphics card instead of one.

316 These optimization mechanisms can be turned on or off at the source code level in
317 GPUMCD.

318 **D. Performance evaluation**

319 The performance evaluation of GPUMCD is twofold: a dosimetric evaluation against
320 EGSnrc/DOSXYZnrc and an efficiency evaluation against EGSnrc and DPM, the later being
321 a fairer comparison since DPM was designed for the same reason GPUMCD was developed,
322 *i.e.* fast MC dose calculations.

323 All settings for DPM were set to default, notably $K_{cut} = 200$ keV and $P_{cut} = 50$ keV.

324 Most parameters for DOSXYZnrc (unless otherwise noted) were also set to default, notably
 325 ESTEPE=0.25, ξ_{max} =0.5. In EGSnrc/DOSXYZnrc, the boundary crossing algorithm used
 326 was PRESTA-I and the electron step algorithm was PRESTA-II, atomic relaxation was turned
 327 off as well as bound Compton scattering. Values of P_{cut} and E_{cut} were set to 0.01 MeV and
 328 0.7 MeV respectively. The same 64^3 grid with 0.5 cm^3 voxels is used for all simulations on
 329 all platforms. These values of spatial resolution and number of voxels are insufficient for a
 330 clinical calculation with patient specific data; however, they were judged adequate for the
 331 benchmarking study conducted here. Preliminary results suggest that no loss of efficiency
 332 occurs between GPUMCD and other platforms as the number of voxels is increased.

333 The uncertainty of Monte Carlo simulation results varies as $1/\sqrt{N}$ where N is the number
 334 of histories. All simulations ran for visualization purposes on GPUMCD were conducted with
 335 enough primary particles to achieve a statistical uncertainty of 1% or less. The same number
 336 of particles were then generated in DOSXYZnrc. The graphs are shown without error bars
 337 since they would simply add clutter to the results. For execution time comparisons, 4 million
 338 particles were generated and simulated for photon beams and 1 million particles for electron
 339 beams. All sources were modeled as a monoenergetic parallel beam. All dose distributions
 340 were normalized with respect to D_{max} . The efficiency measure, ϵ , was used to evaluate the
 341 performance of the different implementations:

$$\epsilon = \frac{1}{s^2 T}, \quad (11)$$

342 where s is the statistical uncertainty and T the computation time. Only voxels with a dose
 343 higher than $0.2 \cdot D_{max}$ were considered for the statistical uncertainty, yielding the following
 344 expression for the uncertainty [45]:

$$s = \frac{1}{N_{0.2}} \sum_{D_{ijk} > 0.2 D_{max}} \frac{\Delta D_{ijk}}{D_{ijk}}, \quad (12)$$

345 where

$$\Delta D_{ijk}^2 = \frac{\langle D_{ijk}^2 \rangle - \langle D_{ijk} \rangle^2}{N - 1}, \quad (13)$$

346 for N the number of histories simulated, $\langle D \rangle$ the mean of the random variable D and $N_{0.2}$
 347 the number of voxel with dose higher than $0.2 D_{max}$.

348 For the dosimetric evaluation, a gamma index was used to compare the two dose distri-
 349 butions [46]. The gamma index for one voxel x is defined as

$$\gamma(x) = \min\{\Gamma(x, x')\} \forall \{x'\}, \quad (14)$$

350 and

$$\Gamma(x, x') = \sqrt{\frac{\|x' - x\|^2}{\Delta d^2} + \frac{|D(x) - D(x')|^2}{\Delta D^2}}, \quad (15)$$

351 where $\|x' - x\|$ is the distance between voxels x and x' , $D(x)$ is the dose value of voxel
 352 x , Δd is the distance tolerance value and ΔD is the dose tolerance value. The criteria for
 353 acceptable calculation is defined for a gamma index value below or equal to 1.0.

354 All simulations were run on the same PC comprising an Intel Core i7 860 and a NVIDIA
 355 GeForce GTX480 graphics card. DPM and DOSXYZnrc do not natively support multi-
 356 core architectures and have not been modified. GPUMCD, unless running in multi-GPU
 357 configuration, uses only one processor core.

358 III. RESULTS

359 Several slab-geometry phantoms are described in Sec. III A . In Sec. III B, the execution
 360 times and gains in efficiency are reported. A multi-GPU implementation is also tested and
 361 corresponding acceleration factors are presented.

362 A. Dosimetric results

363 For slab geometries, central axis percent depth dose (PDD) curves as well as dose profiles
 364 at different depths or isodose curves are presented. Gamma indices are calculated in the
 365 entire volume of voxels and the maximum and average values are reported. The number of
 366 voxels with a gamma value higher than 1.0 and 1.2 are also detailed in order to evaluate
 367 discrepancies in dose calculation. The gamma criteria used is set to 2% and 2 mm which is a
 368 generally accepted criteria for clinical dose calculation [47]. In every gamma index summary
 369 table: 1) γ^{max} is the maximum gamma value for the entire volume of voxel; 2) γ_c^{avg} is the
 370 average gamma value for voxels with $D > cD_{max}$; 3) ΣD_c is the number of voxels with
 371 $D > cD_{max}$; 4) $\Sigma \gamma_c > g$ is the number (proportion) of voxels with $D > cD_{max}$ and $\gamma > g$.

372 The first slab geometry is a simple water phantom. GPUMCD treats homogeneous
 373 phantoms as heterogeneous phantoms; the particles are transported as if evolving inside
 374 a heterogeneous environment and therefore there is no gain in efficiency resulting from
 375 homogeneous media. For this geometry, the results for an electron beam and a photon beam
 376 are presented in Fig. 1 and gamma results in Tab. I.

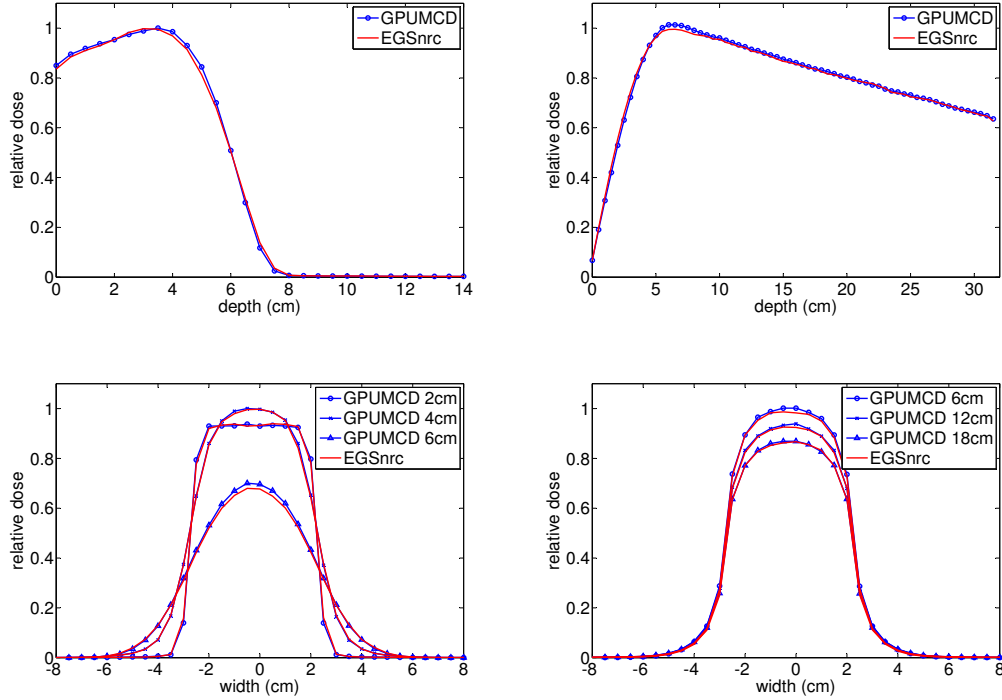


FIG. 1. PDD (top) and profile (bottom) of 15 MeV electron (left) and photon (right) beams on water.

Particles	γ^{max}	$\gamma_{0.2}^{avg}$	$\Sigma D_{0.2}$	$\Sigma \gamma_{0.2} > 1.0$	$\Sigma \gamma_{0.2} > 1.2$
Electrons	1.24	0.29	1750	37 (2%)	2 (~0%)
Photons	1.27	0.18	7500	143 (2%)	19 (~0%)

TABLE I. Gamma criteria summary for a 15 MeV beam on water.

377 The second geometry is composed of a lung box inside a volume of water. It is designed
 378 to demonstrate the performance of GPUMCD with lateral and longitudinal disequilibrium

379 conditions. For electrons, the lung box is 4 cm long, 4.5 cm wide and starts at a depth of
 380 3 cm; for photons the lung box is 6.5 cm long, 4.5 cm wide and starts at a depth of 5.5 cm.
 381 In both cases, the box is centered on the central axis. For this geometry, PDD and isodose
 382 plots are presented in Fig. 2 for the electron and photon beams while the gamma results are
 383 presented in Tab. II.

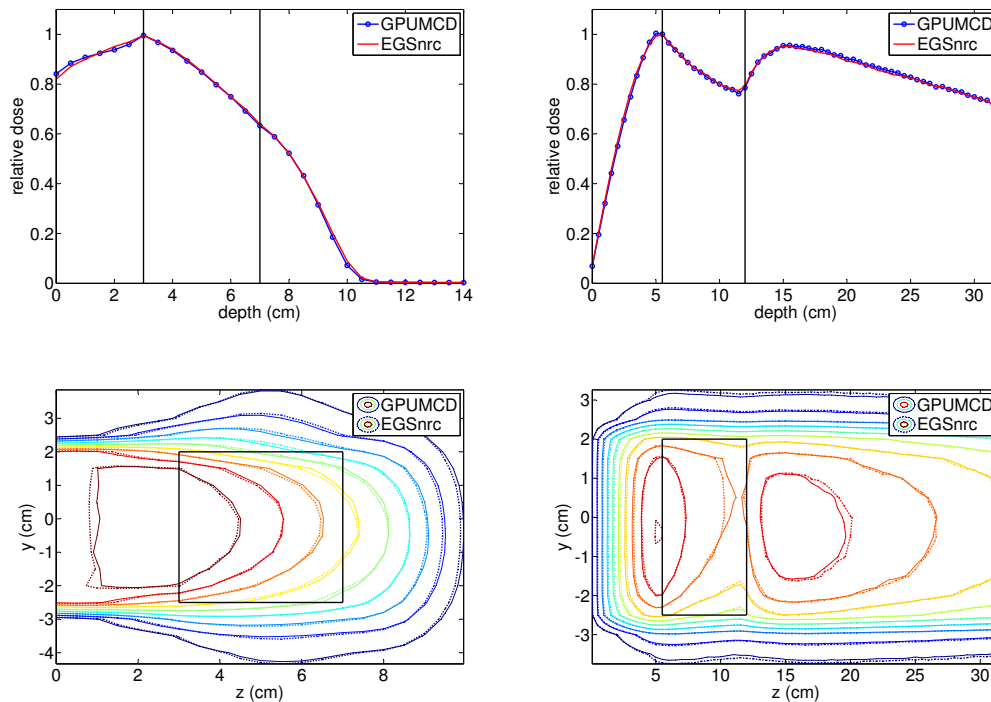


FIG. 2. PDD (top) and isodose (bottom) of a (left) 15 MeV electron beam on water with a 4 cm long, 4.5 cm wide box of lung at a depth of 3 cm and (right) 15 MeV photon beam on water with a 6.5 cm long, 4.5 cm wide box of lung at a depth of 5.5 cm.

Particles	γ^{max}	$\gamma_{0.2}^{avg}$	$\Sigma D_{0.2}$	$\Sigma \gamma_{0.2} > 1.0$	$\Sigma \gamma_{0.2} > 1.2$
Electrons	1.40	0.32	2366	46 (2%)	2 (0%)
Photons	1.30	0.19	7522	122 (2%)	19 (~0%)

TABLE II. Gamma criteria summary for a 15 MeV beam on water with a lung box.

384 The third geometry is composed of soft tissue, bone and lung. The slabs, for electrons,
 385 are arranged as such: 2 cm of soft tissue, 2 cm of lung, 2 cm of bone followed by soft tissue.

386 For photons the geometry is: 3 cm of soft tissue, 2 cm of lung, 7 cm of bone followed by soft
 387 tissue. The results for the electron and photon beams are presented in Fig. 3 and gamma
 388 results in Tab. III.

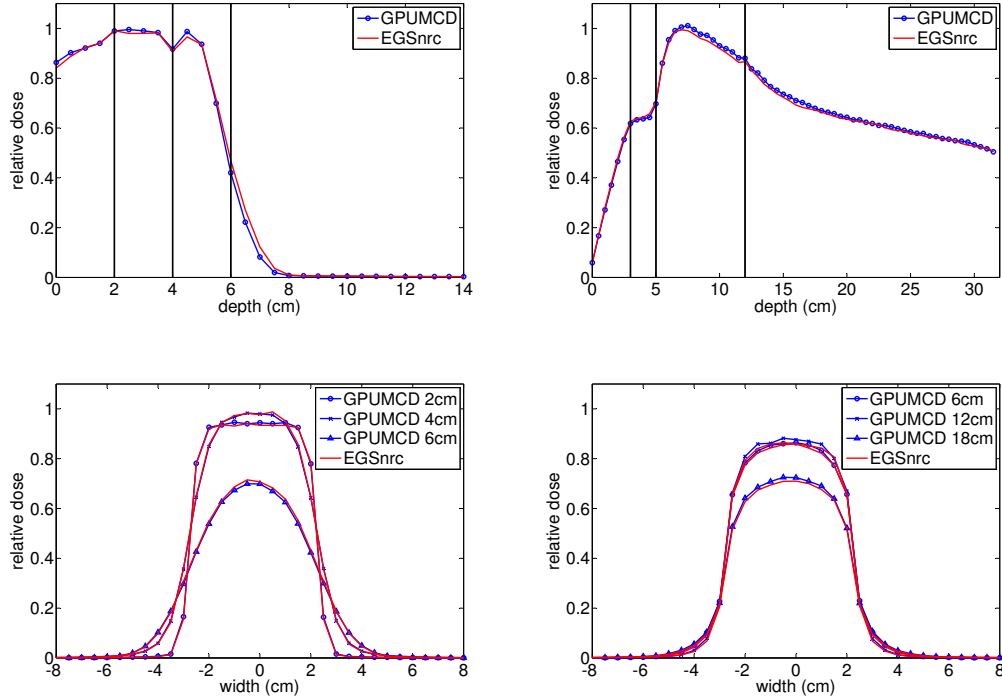


FIG. 3. PDD (top) and profile (bottom) of a (left) 15 MeV electron beam on a phantom composed of 2 cm of soft tissue, 2 cm of bone, 2 cm of lung followed by soft tissue and (right) 15 MeV photon beam on a phantom composed of 3 cm of soft tissue, 2 cm of lung, 7 cm of bone followed by soft tissue.

Particles	γ^{max}	$\gamma_{0.2}^{avg}$	$\Sigma D_{0.2}$	$\Sigma \gamma_{0.2} > 1.0$	$\Sigma \gamma_{0.2} > 1.2$
Electrons	1.84	0.34	1700	138 (8%)	54 (3%)
Photons	1.31	0.22	7220	12 ($\sim 0\%$)	0 (0%)

TABLE III. Gamma criteria summary for a 15 MeV beam on a phantom with layers of soft tissue, bone and lung.

389 **B. Execution time and efficiency gain**

390 In this section, the absolute execution times as well as the overall speed and efficiency of
 391 GPUMCD is evaluated and compared to EGSnrc and DPM. In the following tables, $Geom_1$
 392 is the water phantom, $Geom_2$ is the water-lung phantom and $Geom_3$ is the tissue-lung-bone
 393 phantom. T_{EGSnrc} and T_{DPM} are respectively the EGSnrc and DPM execution times. For
 394 the efficiency measurement, ϵ , the fastest execution time of GPUMCD (with or without the
 395 optimization presented in Sec. II C 3) has been used. The acceleration factor and efficiency
 396 improvement, namely A and A_ϵ , also use the fastest time for GPUMCD. The acceleration
 397 factor is defined as

$$A = \frac{T_{ref}}{T_{GPUMCD}}, \quad (16)$$

398 and the efficiency improvement as

$$A_\epsilon = \frac{\epsilon_{GPUMCD}}{\epsilon_{ref}}. \quad (17)$$

399 Tab. IV presents the absolute execution times for all simulations with both electron and
 400 photon beams.

Particles	$Geom_1$	$Geom_2$	$Geom_3$
	(seconds)		
Electrons	0.118	0.147	0.162
Photons	0.269	0.275	0.366

TABLE IV. Absolute execution times, in seconds, for GPUMCD in the three geometries for 1M electrons and 4M photons using 15 MeV monoenergetic beams.

401 Tab. V presents the acceleration results for photon and electron beams where 4M photons
 402 and 1M electrons are simulated.

403 Tab. VI presents the results of the divergence reduction methods and acceleration strate-
 404 gies presented in Sec. II C 3 for electron and photon beams. In the following table A_{comp} ,
 405 A_{pool} represent the acceleration factors with respect to the base configuration execution
 406 time (T_{base}), with the stream compaction or *pool* divergence reduction methods enabled,
 407 respectively.

		Photons		Electrons	
		DPM	EGSnrc	DPM	EGSnrc
$Geom_1$	A	453	1161	246	1510
	A_e	515	1174	291	1740
$Geom_2$	A	433	1058	210	1264
	A_e	474	1305	237	1403
$Geom_3$	A	203	947	225	1231
	A_e	220	1050	242	1359

TABLE V. Acceleration factors for 1M 15 MeV electrons and 4M 15 MeV photons on the three geometries presented. Absolute execution times of 0.269 s, 0.275 s and 0.366 s were found with GPUMCD for $Geom_1$, $Geom_2$ and $Geom_3$ respectively for a photon beam and 0.118 s, 0.147 s and 0.162 s for an electron beam.

Particles	T_{base}	A_{comp}	A_{pool}
Electrons	0.185	1.06	1.26
Photons	0.275	0.85	0.98

TABLE VI. Acceleration results of the different strategies presented in Sec. II C 3 for the second geometry ($geom_2$).

408 As detailed in Sec. II C 3, GPUMCD can take advantage of a system with multiple GPUs.
409 The impact of parallelizing GPUMCD on two GPUs is presented in Tab. VII where TPH
410 (time per history) is the execution time normalized to one complete history including a
411 primary particle and all its secondary particles, TPH_s and TPH_d are the execution time in
412 single and dual GPU mode, respectively. The graphics cards used for this test are a pair of
413 Tesla C1060. The reported execution times include every memory transfer to and from the
414 graphics cards.

	TPH_s	TPH_d	$A_{d/s}$
	(μs)	(μs)	
Electrons	5.43	2.82	1.92
Photons	5.20	2.74	1.90

TABLE VII. Execution times and acceleration factors achieved with a multi-GPU configuration.

415 IV. DISCUSSION

416 A. Dosimetric evaluation

417 Figures 1 - 3 and Tables I - III present the dosimetric evaluation performed between
 418 GPUMCD and EGSnrc. An excellent agreement is observed for homogeneous phantoms
 419 with both photon and electron beams, except for the end of the build-up region where small
 420 differences of less than 2% can be observed. In both cases, the rest of the curve as well as
 421 the overall range of the particles are not affected.

422 In heterogeneous simulations with low density materials, the agreement is also excellent.
 423 Differences of up to 2% can be seen in the build-up region for an incoming electron beam.
 424 These differences again do not affect the range of the particles. For a photon beam imping-
 425 ing on the water-lung phantom, the dose is in good agreement within as well as near the
 426 heterogeneity.

427 In heterogeneous simulations with a high-Z material, differences of up to 2% are found
 428 with an impinging electron beam and no differences above 1% are found for the photon
 429 beam in the presented PDD while differences of up to 1.5% are found in the profiles.

430 The overall quality of the dose comparison can be evaluated with the gamma value results
 431 presented in Tab. I to III. Results suggest that the code is suitable for clinical applications
 432 as the dose accuracy is within the 2%/2 mm criteria, for all cases but one, which is below
 433 the recommended calculation accuracy proposed by Van Dyk [47]. For electron beams, the
 434 gamma criteria has been well respected in the first two geometries where at most 2% of the
 435 significant voxels failed. More pronounced differences have been found in the last geometry
 436 including a high-Z material where 8% of the significant voxels fail the gamma test. However,
 437 only 3% of all significant voxels fail that test with a value higher than 1.2, indicating that

438 the criteria are slightly too strict. Indeed, with a 2.5%-2.5mm, 3% of all significant voxels
439 fail the test. For photon beams, all geometries meet the gamma criteria for 98 % or more
440 of all significant voxels.

441 B. Execution times

442 The differences in calculation efficiency between GPUMCD and the other two codes
443 are due to three distinctive reasons: 1) differences in hardware computational power, 2)
444 differences in the programming model and its adaptation to hardware and 3) differences
445 in the physics simulated and approximations made. As an operation-wise equivalent CPU
446 implementation of GPUMCD does not exist, these factors cannot be evaluated individually.

447 Also, the simulation setup for the test cases uses monoenergetic beams, which can favor
448 GPU implementations. A naive GPU implementation of polyenergetic beams would lead
449 to additional stream divergence. However, simple measures such as grouping particles with
450 similar energy values would reduce this divergence. Future work will explore this issue in
451 the context of clinical calculations done with polyenergetic beams.

452 Tab. IV shows the absolute execution times for electron and photon beams with GPUMCD.
453 Execution times of less than 0.2 s are found for all electron cases. The execution time is
454 higher in the simulation with lung when compared to the simulation in water likely due to
455 the fact that more interactions are necessary. The execution time is higher in the simulation
456 with bone because a larger number of fictitious interactions will be encountered. Similar
457 conclusions can be taken in the cases with photon beams in which the first two simulations
458 require less than 0.3 s and the simulation with a bone slab required more than 0.36 s.

459 Tab. V shows the acceleration results comparing GPUMCD to DPM and EGSnrc. It
460 can be seen that GPUMCD is consistently faster than DPM, by a factor of at least 203x
461 for photon beams and 210x for electron beams. The disadvantage of using the Woodcock
462 raytracing algorithm is apparent in Tab V where the geometry featuring a heavier than
463 water slab has the lowest acceleration factor. An acceleration of more 1200x is observed
464 when comparing to EGSnrc for both electron beams and more than 940x for photon beams.

465 DPM and EGSnrc both employ much more sophisticated electron step algorithms com-
466 pared to GPUMCD. Improvements to the electron-step algorithm in GPUMCD will most
467 likely yield greater accelerations, as photon transport was shown to be much faster than the

468 reported coupled transport results [48], as well as improved dosimetric results.

469 Tab. VI presents the execution times and acceleration factors for the different divergence
470 reduction methods and optimizations presented in Sec. II C 3. Gains of up to 26% for
471 electron beams are observed. However, acceleration factors below 1 are found for photon
472 beams, showing that electron beams are more divergent. These results show that the GPU
473 architecture is not ideal for Monte Carlo simulations but that the hardware is able to cope
474 well with this divergence. The mechanisms employed in GPUMCD to reduce this penalty
475 have either had a negative impact on the execution time or a small positive impact that is
476 perhaps not worth the loss in code readability and maintainability.

477 Tab. VII details the gain that can be obtained by executing GPUMCD on multiple
478 graphics card. GPUMCD presents a linear growth with respect to the number of GPUs.
479 This is expected as there is a relatively small amount of data transferred to the GPUs
480 compared to the amount of computations required in a typical simulation. As the number
481 of histories is reduced, so is the acceleration factor.

482 Efficiency improvements can be achieved with variance reduction techniques (VRT). Sev-
483 eral methods have been published to improve the calculation efficiency of EGSnrc for in-
484 stance [2, 49]. A fair comparison of GPUMCD with other Monte Carlo packages would
485 ideally involve an optimal usage of the codes. In this paper, no VRT was used for the
486 comparisons. It is not clear yet how VRT could potentially be implemented in GPUMCD.
487 In the eventuality that VRT are equally applicable to each code architecture, the efficiency
488 improvements reported in this paper would remain roughly the same. Otherwise, GPUMCD
489 might suffer from a performance penalty compared to VRT-enabled codes.

490 V. CONCLUSION AND FUTURE WORK

491 In this paper, a new fully coupled GPU-oriented Monte Carlo dose calculation platform
492 was introduced. The accuracy of the code was evaluated with various geometries and com-
493 pared to EGSnrc, a thoroughly validated Monte Carlo package. The overall speed of the
494 platform was compared to DPM, an established fast Monte Carlo simulation package for
495 dose calculations. For a 2%-2mm gamma criteria, the dose comparison is in agreement for
496 98% or more of all significant voxels, except in one case: the tissue-bone-lung phantom with
497 an electron beam where 92% of significant voxels pass the gamma criteria. These results

498 suggest that GPUMCD is suitable for clinical use.

499 The execution speed achieved by GPUMCD, at least two orders of magnitude faster than
500 DPM, let envision the use of accurate of Monte Carlo dose calculations for numerically
501 intense applications such as IMRT or arc therapy optimizations. A 15 MeV electron beam
502 dose calculation in water can be performed in less than 0.12 s for 1M histories while a photon
503 beam calculation takes less than 0.27 s for 4M histories.

504 GPUMCD is currently under active development. Future work will include the ability
505 to work with phase space and spectrum files as well as the integration and validation of
506 CT-based phantoms for dose calculation. Research towards variance reduction techniques
507 that are compatible with the GPU architecture is also planned.

508 ACKNOWLEDGMENT

509 This work was supported by Natural Sciences and Engineering Research Council of
510 Canada (NSERC). Dual GPU computations were performed on computers of the Réseau
511 québécois de calcul de haute performance (RQCHP). Multiple scattering data has been
512 provided by the National Research Council of Canada (NRC).

513 REFERENCES

-
- 514 [1] W.R. Nelson, H. Hirayama, and D.W.O. Rogers. The EGS4 code system. *SLAC-265, Stanford*
515 *Linear Accelerator Center*, 1985.
- 516 [2] I. Kawrakow. Accurate condensed history Monte Carlo simulation of electron transport. I.
517 EGSnrc, the new EGS4 version. *Medical Physics*, 27(3):485–498, 2000.
- 518 [3] I. Kawrakow and DWO Rogers. PIRS-701: The EGSnrc Code System: Monte Carlo Simulation
519 of Electron and Photon Transport. *Ionizing Radiation Standards (NRC, Ottawa, Ontario,*
520 *2003)*, 2003.
- 521 [4] H. Hirayama, Y. Namito, W.R. Nelson, A.F. Bielajew, and S.J. Wilderman. *The EGS5 code*
522 *system*. United States. Dept. of Energy, 2005.

- 523 [5] F. Salvat, J.M. Fernández-Varea, and J. Sempau. PENELOPE-2006: a code system for Monte
524 Carlo simulation of electron and photon transport. In *OECD/NEA Data Bank*, 2006. Available
525 at <http://www.nea.fr/science/pubs/2006/nea6222-penelope.pdf>.
- 526 [6] J. Baro, J. Sempau, JM Fernandez-Varea, and F. Salvat. PENELOPE: an algorithm for
527 Monte Carlo simulation of the penetration and energy loss of electrons and positrons in mat-
528 ter. *Nuclear Instruments and Methods in Physics Research Section B: Beam Interactions with*
529 *Materials and Atoms*, 100(1):31–46, 1995.
- 530 [7] DWO Rogers. Fifty years of Monte Carlo simulations for medical physics. *Physics in medicine*
531 *and biology*, 51:R287, 2006.
- 532 [8] R. Mohan, C. Chui, and L. Lidofsky. Differential pencil beam dose computation model for
533 photons. *Medical Physics*, 13(1):64–73, 1986.
- 534 [9] Anders Ahnesjö, Mikael Saxner, and Avo Trepp. A pencil beam model for photon dose calcu-
535 lation. *Medical Physics*, 19(2):263–273, 1992.
- 536 [10] U Jelen, M Söhn, and M Alber. A finite size pencil beam for IMRT dose optimization. *Physics*
537 *in Medicine and Biology*, 50(8):1747, 2005.
- 538 [11] T. R. Mackie, J. W. Scrimger, and J. J. Battista. A convolution method of calculating dose
539 for 15-MV x rays. *Medical Physics*, 12(2):188–196, 1985.
- 540 [12] H. Helen Liu, T. Rock Mackie, and Edwin C. McCullough. A dual source photon beam model
541 used in convolution/superposition dose calculations for clinical megavoltage x-ray beams. *Med-*
542 *ical Physics*, 24(12):1960–1974, 1997.
- 543 [13] T. Krieger and O.A. Sauer. Monte Carlo-versus pencil-beam-/collapsed-cone-dose calculation
544 in a heterogeneous multi-layer phantom. *Physics in medicine and biology*, 50:859, 2005.
- 545 [14] George X. Ding, Joanna E. Cygler, Christine W. Yu, Nina I. Kalach, and G. Daskalov. A
546 comparison of electron beam dose calculation accuracy between treatment planning systems
547 using either a pencil beam or a Monte Carlo algorithm. *International Journal of Radiation*
548 *Oncology Biology Physics*, 63(2):622 – 633, 2005.
- 549 [15] C-M Ma, T Pawlicki, S B Jiang, J S Li, J Deng, E Mok, A Kapur, L Xing, L Ma, and A L
550 Boyer. Monte Carlo verification of IMRT dose distributions from a commercial treatment
551 planning optimization system. *Physics in Medicine and Biology*, 45(9):2483, 2000.
- 552 [16] Iwan Kawrakow, Matthias Fippel, and Klaus Friedrich. 3D electron dose calculation using a
553 Voxel based Monte Carlo algorithm (VMC). *Medical Physics*, 23(4):445–457, 1996.

- 554 [17] Matthias Fippel. Fast Monte Carlo dose calculation for photon beams based on the VMC
555 electron algorithm. *Medical Physics*, 26(8):1466–1475, 1999.
- 556 [18] J. Gardner, J. Siebers, and I. Kawrakow. Dose calculation validation of VMC++ for photon
557 beams. *Medical Physics*, 34(5):1809–1818, 2007.
- 558 [19] Josep Sempau, Scott J Wilderman, and Alex F Bielajew. DPM, a fast, accurate Monte Carlo
559 code optimized for photon and electron radiotherapy treatment planning dose calculations.
560 *Physics in Medicine and Biology*, 45(8):2263–2291, 2000.
- 561 [20] O. Kutter, R. Shams, and N. Navab. Visualization and GPU-accelerated simulation of medical
562 ultrasound from CT images. *Computer methods and programs in biomedicine*, 94(3):250–266,
563 2009.
- 564 [21] M. de Greef, J. Crezee, J. C. van Eijk, R. Pool, and A. Bel. Accelerated ray tracing for
565 radiotherapy dose calculations on a GPU. *Medical Physics*, 36(9):4095–4102, 2009.
- 566 [22] Sami Hissoiny, Benoît Ozell, and Philippe Després. A convolution-superposition dose calcula-
567 tion engine for GPUs. *Medical Physics*, 37(3):1029–1037, 2010.
- 568 [23] X. Jia, Y. Lou, R. Li, W.Y. Song, and S.B. Jiang. GPU-based fast cone beam CT reconstruction
569 from undersampled and noisy projection data via total variation. *Medical physics*, 37:1757,
570 2010.
- 571 [24] Vasily Volkov and James W. Demmel. Benchmarking GPUs to tune dense linear algebra.
572 In *SC '08: Proceedings of the 2008 ACM/IEEE conference on Supercomputing*, pages 1–11,
573 Piscataway, NJ, USA, 2008. IEEE Press.
- 574 [25] J.A. Anderson, C.D. Lorenz, and A. Travasset. General purpose molecular dynamics simu-
575 lations fully implemented on graphics processing units. *Journal of Computational Physics*,
576 227(10):5342–5359, 2008.
- 577 [26] S. Chen, J. Qin, Y. Xie, J. Zhao, and P.A. Heng. A fast and flexible sorting algorithm with
578 cuda. *Algorithms and Architectures for Parallel Processing*, pages 281–290, 2009.
- 579 [27] T. Preis, P. Virnau, W. Paul, and J.J. Schneider. GPU accelerated Monte Carlo simulation of
580 the 2D and 3D Ising model. *Journal of Computational Physics*, 228(12):4468–4477, 2009.
- 581 [28] M. Januszewski and M. Kostur. Accelerating numerical solution of stochastic differential equa-
582 tions with CUDA. *Computer Physics Communications*, 181(1):183–188, 2010.
- 583 [29] Erik Alerstam, Tomas Svensson, and Stefan Andersson-Engels. Parallel computing with graph-
584 ics processing units for high-speed Monte Carlo simulation of photon migration. *Journal of*

- 585 *Biomedical Optics*, 13(6):060504, 2008.
- 586 [30] Andreu Badal and Aldo Badano. Accelerating Monte Carlo simulations of photon transport
587 in a voxelized geometry using a massively parallel graphics processing unit. *Medical Physics*,
588 36(11):4878–4880, 2009.
- 589 [31] Xun Jia, Xuejun Gu, Josep Sempau, Dongju Choi, Amitava Majumdar, and Steve B Jiang.
590 Development of a GPU-based Monte Carlo dose calculation code for coupled electron-photon
591 transport. *Physics in Medicine and Biology*, 55(11):3077, 2010.
- 592 [32] L. L. Carter, E. D. Cashwell, and W. M. Taylor. Monte Carlo Sampling with Continuously
593 Varying Cross Sections Along Flight Paths. *Nucl. Sci. Eng.*, 48:403–411, 1972.
- 594 [33] O. Klein and T. Nishina. Uber die Streuung von Strahlung durch freie Elektronen nach
595 der neuen relativistischen Quantendynamik von Dirac. *Zeitschrift fur Physik A Hadrons and*
596 *Nuclei*, 52(11):853–868, 1929.
- 597 [34] CJ Everett, ED Cashwell, and GD Turner. A new method of sampling the Klein-Nishina
598 probability distribution for all incident photon energies above 1 keV. Technical report, LA-
599 4663, Los Alamos Scientific Lab., N. Mex., 1971.
- 600 [35] Harold Elford Johns and John Robert Cunningham. *The Physics of Radiology, fourth edition*,
601 page 181. Charles C Thomas, Springfield IL, 1983.
- 602 [36] F. Sauter. Atomic photoelectric effect in the K-shell according to the relativistic wave mecha-
603 nisms of Dirac. *Ann. Phys.(Leipzig)*, 11:454–488, 1931.
- 604 [37] I. Kawrakow and DWO Rogers. The EGSnrc code system: Monte Carlo simulation of electron
605 and photon transport, NRCC Report PIRS-701. *Ottawa (ON): National Research Council of*
606 *Canada*, 2006.
- 607 [38] M.J. Berger. Monte Carlo calculation of the penetration and diffusion of fast charged particles.
608 *Methods in computational physics*, 1:135–215, 1963.
- 609 [39] Iwan Kawrakow and Alex F. Bielajew. On the representation of electron multiple elastic-
610 scattering distributions for Monte Carlo calculations. *Nuclear Instruments and Methods in*
611 *Physics Research Section B: Beam Interactions with Materials and Atoms*, 134(3-4):325 – 336,
612 1998.
- 613 [40] Sami Hissoiny, Benoît Ozell, and Philippe Després. Fast convolution-superposition dose cal-
614 culation on graphics hardware. *Medical Physics*, 36(6):1998–2005, 2009.

- 615 [41] George Marsaglia and Arif Zaman. A New Class of Random Number Generators. *The Annals*
616 *of Applied Probability*, 1(3):462-480, 1991.
- 617 [42] Pierre L'ecuyer and Richard Simard. TestU01: A C library for empirical testing of random
618 number generators. *ACM Trans. Math. Softw.*, 33(4):22, 2007.
- 619 [43] M. Billeter, O. Olsson, and U. Assarsson. Efficient stream compaction on wide SIMD many-
620 core architectures. In *Proceedings of the 1st ACM conference on High Performance Graphics*,
621 pages 159–166. ACM, 2009.
- 622 [44] Timo Aila and Samuli Laine. Understanding the Efficiency of Ray Traversal on GPUs. In
623 *Proc. High-Performance Graphics*, 2009.
- 624 [45] I. Kawrakow and M. Fippel. Investigation of variance reduction techniques for Monte Carlo
625 photon dose calculation using XVMC. *Physics in medicine and biology*, 45:2163, 2000.
- 626 [46] Daniel A. Low and James F. Dempsey. Evaluation of the gamma dose distribution comparison
627 method. *Medical Physics*, 30(9):2455–2464, 2003.
- 628 [47] J. Van Dyk et al. *The modern technology of radiation oncology*, pages 252–253. Medical Physics
629 Publ., 1999.
- 630 [48] Sami Hissoiny, Benoît Ozell, and Philippe Després. GPUMCD, a new GPU-oriented Monte
631 Carlo dose calculation platform. In *XVIth ICCR Conference Proceedings*, 31 May - 3 June
632 2010. Amsterdam, NL.
- 633 [49] J. Wulff, K. Zink, and I. Kawrakow. Efficiency improvements for ion chamber calculations in
634 high energy photon beams. *Medical physics*, 35:1328, 2008.